Journal of Southeast University (English Edition) Vol. 34, No. 2, pp. 220 - 228 June 2018 ISSN 1003—7985

Experimental study on axial compressive behaviors of prefabricated composite thermal insulation walls after single-side fire exposure

Fu Qian[1] Zhu Xiaojun[2] Liang Shuting[1] Yang Jian[1] Li Xiangmin[3] Xu Qingfeng[3] Gao Mingzhu[1]

([1]School of Civil Engineering, Southeast University, Nanjing 210096, China)
([2] Architects & Engineers Co., Ltd., Southeast University, Nanjing 210096, China)
([3]Shanghai Key Laboratory of Engineering Structure Safety,
Shanghai Research Institute of Building Sciences, Shanghai 200032, China)

Abstract: The axial bearing capacity of prefabricated composite walls composed of inner and outer concrete wythes, expandable polystyrene (EPS) boards and steel sleeve connectors is investigated. An experimental study on the axial bearing capacity of four prefabricated composite walls after fire treatment is carried out. Two of the prefabricated composite walls are normal-temperature specimens, and the others are treated with fire. The damage modes and crack development are observed, and the axial bearing capacity, lateral deformation of the specimens, and the concrete and reinforcing bar strain are tested. The results show that the ultimate bearing capacity of specimens after a fire is less than that of normal-temperature specimens; when the insulation board thicknesses are 40 mm and 60 mm, the decrease amplitudes are 20.8% and 16.8%, respectively. The maximum lateral deformation of specimens after a fire is greater than that of normal-temperature specimens, and under the same level of load, the lateral deformation increases as the insulation board thickness increases. Moreover, the strain values of the concrete and reinforcing bars of specimens after a fire are greater than those of normal-temperature specimens, and the strain values increase as the thickness of insulation board increases.

Key words: prefabricated composite thermal insulation walls; expandable polystyrene board; fire exposure; insulation layer; post-fire; axial compressive behavior

DOI: 10.3969/j.issn.1003-7985.2018.02.012

Over the past few decades, the demand for ecofriendly, lightweight, durable structural systems has increased. Prefabricated composite thermal insulation walls, which are composed of inner and outer concrete wythes surrounded by a central layer of foam insulation with reasonable thermal performance, play a role in energy savings, as the flow of heat from the interior to the outside environment can be prevented by the built-in insulation layer. A very signifant number of scholars have conducted research on prefabricated composite thermal insulation walls. Mousa and Uddin[1] investigated the structural behavior of insulated wall panels under eccentric loading and proposed an analytical model to justify the observed wrinkling failure mode. Mathieson and Fam[2] studied the influence of the slenderness ratio on the axial compressive properties of sandwich walls. The results showed that the axial load capacity and observed failure modes of the sandwich walls were correlated with the slenderness ratio as well as the nature of the sandwich walls, namely, the internal ribs. The structural performance of sandwich walls subjected to concentric axial loads was studied by Abdolpour et al[3]. The linear elastic response of wall panels was observed prior to failure through the analysis of load-mid-height deflection and load-axial displacement curves. Additionally, the characteristics and properties of shear connections[4], the bending behavior[5-6], the effect of cyclic loading[7-9] and the shaking-table response[10] of concrete sandwich walls and composite insulation walls have been studied by different researchers. Summarizing these findings, the mechanical properties of concrete sandwich walls and composite insulation walls were found to be comparable with those of common reinforced concrete walls in terms of design and construction.

Apart from the mechanical properties at ambient temperature, the behavior of composite insulation walls exposed to fires has attracted attention, and a number of studies have been performed. Woltman et al.[11] tested a structural sandwich panel, consisting of a combination of concrete, insulation and connectors, using a hot box apparatus to evaluate its thermal properties and energy efficiency. The results indicated that the thermal conductivity of the internal insulation foam layer has an extremely important influence on the fire resistance of the wall. Zhang et al.[12] analyzed and compared the thermal performance of gypsum plaster, glass magnesium and light-

Received 2018-01-05, **Revised** 2018-04-13.

Biographies: Fu Qian (1988—), female, Ph. D. candidate; Zhu Xiaojun (corresponding author), male, doctor, professor-level senior engineer, 496380566@qq.com.

Foundation items: The National Key Research and Development Program of China (No. 2016YFC0701703), the Natural Science Foundation of Higher Education Institutions of Jiangsu Province (No. 2016TM045J), the Scientific Innovation Research of Graduate Students in Jiangsu Province (No. KYLX_0151).

Citation: Fu Qian, Zhu Xiaojun, Liang Shuting, et al. Experimental study on axial compressive behaviors of prefabricated composite thermal insulation walls after single-side fire exposure[J]. Journal of Southeast University (English Edition), 2018, 34(2): 220-228. DOI: 10.3969/j.issn.1003-7985.2018.02.012.

weight calcium silicate and showed that glass magnesium provided the best fire insulation performance. Pereira et al.[13] tested and evaluated the fire resistance of concrete sandwich wall assemblies and found that a viscous black substance was left after the PET foam melted, while EPS foam left no residue after complete thermal decomposition. Three shear walls with high-strength concrete and a prefabricated recycled concrete wall panel under low cyclic loads after fire treatment made by Xiao et al.[14] showed that spalling of the concrete could be reduced by more than 60% by using recycled concrete panels. Another study conducted by Xiao et al.[15] showed that the seismic behavior of concrete walls deteriorated with fire exposure. Research on fire resistance and structural behavior done by Go et al.[16] demonstrated that lightweight concrete walls were better than normal weight concrete walls in terms of the cracking load, yielding load, ultimate load, stiffness and ductility. Fernando et al.[17] investigated the structural feasibility of expanded polystyrene (EPS)-based lightweight concrete sandwich wall panels and demonstrated that the EPS-based walls can be used as load bearing walls in single-story and multistory construction.

Composite insulation walls need to retain structural safety after being exposed to fires to prevent the failure of vertical load-bearing components. As the relevant research on the mechanical properties of composite insulation walls after fires is insufficient, further research needs to be conducted. In this paper, an experimental study of the axial compressive behaviors of prefabricated composite thermal insulation walls after being exposed to fire on one side are presented. The crack patterns, failure characteristics, ultimate bearing capacity, load-displacement curves and strains of concrete and steel bars will be investigated and evaluated.

1 Experimental Program

1.1 Preparation of specimens

In total, four full-scale specimens of prefabricated composite thermal insulation walls composed of inner and outer concrete wythes surrounding a central layer of expandable polystyrene (EPS) board were tested to investigate their post-fire axial compressive behaviors. All specimens have the same geometrical dimensions of 1 700 mm (width) × 240 mm (thickness) × 2 500 mm (height) and were built with 100 mm × 240 mm embedded columns. The thickness of the insulation layer, however, differs by 40 mm for DW1 and DW2 and 60 mm for DW3 and DW4. The configurations of the reinforcement and stirrup of the walls are Φ8@200 (the diameter of the steel bar is 8 mm, and the interval is 200 mm) and Φ8@100, respectively, and the reinforcement used in the embedded columns is 4 Φ16 (4 steel bars 16 mm in the diameter). The dimensions and reinforcement details of the specimens are shown in Fig. 1. DW1 and DW3 are specimens at room temperature, and DW2 and DW4 are specimens subjected to fire exposure on one side of the wall (The fire exposure time is 120 min following the ASTM E119 standard). The details of each specimen are shown in Tab. 1.

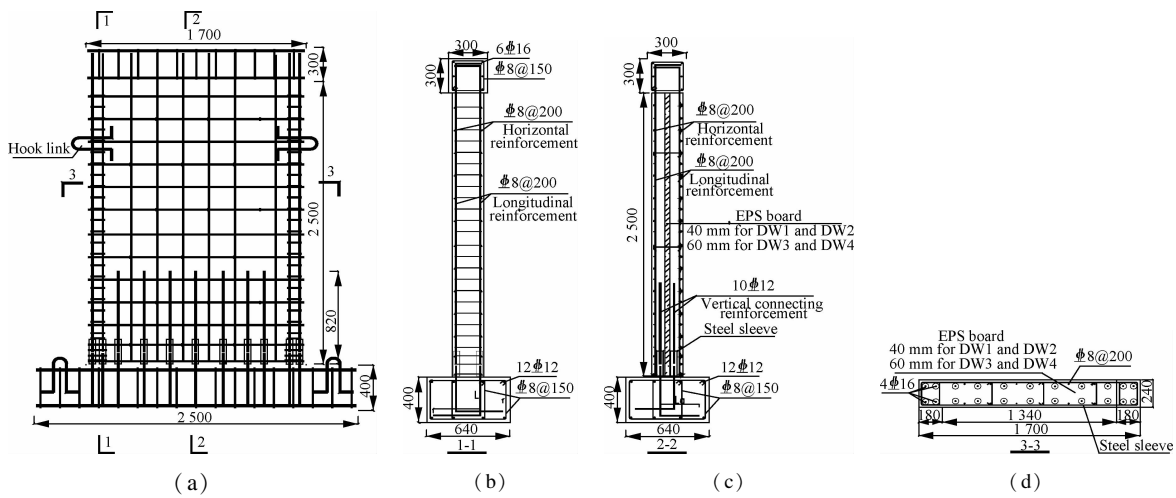

Fig. 1 The dimensions of specimens and the reinforcement details (unit: mm). (a) Specimens dimension and reinforcement; (b) Section 1-1; (c) Section 2-2; (d) Section 3-3

The mechanical properties of the steel bars were determined by tension tests. Tab. 2 shows the measured average yield strength f_y, tensile strength f_u and modulus of elasticity E_s of the steel reinforcement. In addition, three concrete cubic specimens with dimensions of 150 mm × 150 mm × 150 mm were cast in steel molds and cured in the surrounding environment together with the concrete sandwich walls. According to the test results from the hydraulic testing machine, the average compressive strength of the concrete cubes is 27.7 MPa.

One side of the prefabricated composite insulation wall was cast in advance, and the insulation layer was placed

Tab. 1 The details of each specimen

Specimen	Fire exposure time/min	Axial compression ratio	Thickness of EPS board/mm	Horizontal reinforcement ratio ρ_h/%	Vertical reinforcement ratio ρ_v/%
DW1			40	0.16	0.13
DW2	120	0.2	40	0.16	0.13
DW3			60	0.16	0.13
DW4	120	0.2	60	0.16	0.13

Tab. 2 The mechanical properties of reinforcement at room temperature

Diameter/mm	Yield strength f_y/MPa	Tensile strength f_u/MPa	Modulus of elasticity E_s/GPa
8	456.3	601.0	200
16	431.4	576.0	203
18	474.4	614.9	206

in the predetermined position after the initial solidification of the concrete. Then, the other side of the wall was cast. At the top of each specimen, a concrete beam was cast monolithically with the wall to facilitate the application of the axial compressive load. A rigid basement was also cast to fix the specimen to the laboratory floor, simulating a rigid foundation during the test. The prefabricated wall piers and the basements were cast separately and then cured for 28 d. The reinforcement in the wall piers and the basements were connected using steel sleeves[18] in the vertical direction, and the expansive cement mortar was injected.

1.2 Items of investigation

A number of strain gauges with an electric resistance of 120 Ω were attached to the concrete and the reinforcing steel bars in the walls to obtain the strain of each specimen during loading. For specimens DW1 and DW3, which were specimens at room temperature, the strain gauges on the vertical reinforcement were pasted before the concrete was cast. For specimens DW2 and DW4, which were subjected to fire exposure on one side, the concrete cover for the steel bars needed to be removed after exposure to fire before the strain gauges on the vertical reinforcement were pasted. The arrangements of reinforcement and concrete strain gauges are shown in Figs. 2(a) and (b). Three linear variable differential transformers (LVDTs) were installed at the top, middle and bottom of the concrete sandwich wall to measure the out-of-plane displacements, as shown in Fig. 2(c). The axial load of each specimen can be recorded by the hydraulic actuator system. The values of the strain and deformation measured by the strain gauges and the LVDTs were stored in the computer-based data acquisition software. During loading, the width of the concrete crack was measured by a crack observer, and the length was measured with a ruler.

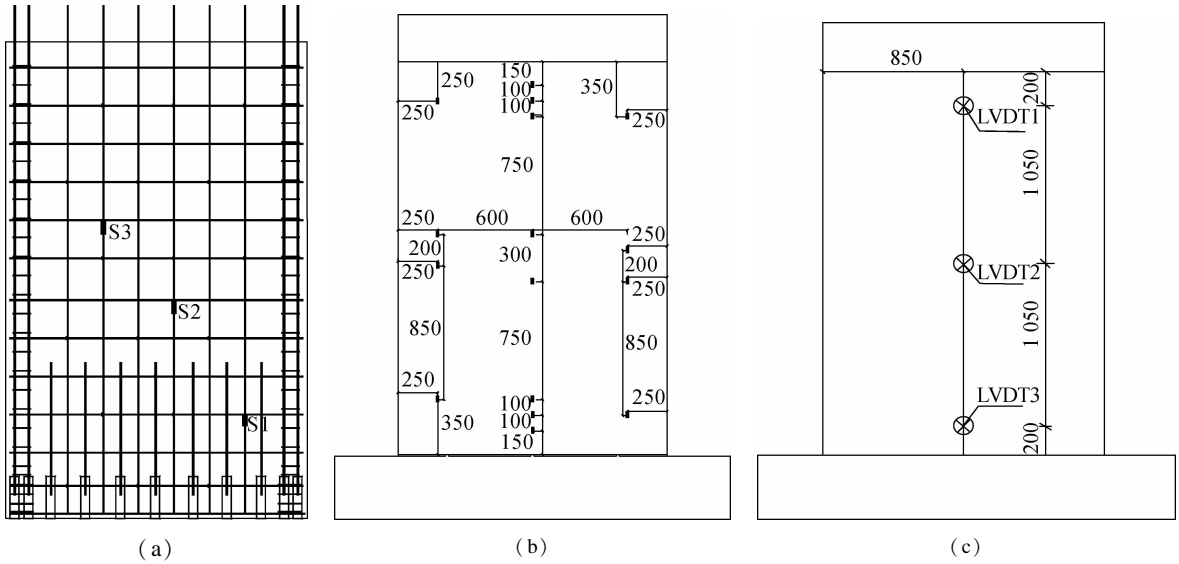

(a) (b) (c)

Fig. 2 The arrangement of strain gauges and LVDTs (unit: mm). (a) Reinforcement strain gauges; (b) Concrete strain gauges; (c) LVDTs

1.3 Test setup and procedure

Specimens DW2 and DW4 were placed horizontally in the fire furnace and exposed to fire on one side with no restraint applied to their other sides (see Figs. 3(a)). When the exposure time (120 min) was reached, the furnace was closed while the ventilator circulated air until the temperature in the chamber dropped below 300 ℃. Then, the heated walls were cooled in a natural environment. Afterwards, a vertical load was applied to the specimen via a hydraulic actuator (whose bearing capacity was 10 MN) fixed on a steel frame, as shown in Fig. 3(b). A steel beam with a large rigidity was fixed to the top of the wall as a loading beam, which subjected the sandwich wall to a uniform load to avoid local crushing of the concrete at the top of the wall. Moreover, steel pipe scaffoldings were located around the specimen to prevent lateral instability and ensure the safety of the researchers

and the instruments. The specimens were preloaded using hierarchical loading. The loading of each stage was approximately 5% of the theoretical value of the ultimate bearing capacity. Then, 10% of the theoretical value of the ultimate bearing capacity was taken, and 5% was once again taken when close to the ultimate bearing capacity. Finally, the loading program was conducted under vertical displacement control, and the test was stopped when the applied load decreased to 85% of the ultimate load.

(a)

(b)

Fig. 3 Schematic of the heating and loading devices. (a) Heating device; (b) Loading device

2 Test Results and Discussion

2.1 Crack patterns and failure characteristics

For specimen DW1, which is a normal-temperature specimen with an insulation thickness of 40 mm, the first crack appeared in the top concrete beam under a load of 800 kN. Vertical cracks in the upper part of the wall occurred under a loading level of 2 000 kN. When the load reached 3 600 kN, vertically penetrating cracks were observed at both ends of the wall, and a number of transverse cracks were found at the top of the wall. With the increase in external loading, a number of new cracks appeared, and both the length and width of the original cracks became larger. The ultimate load was obtained when the out-of-plane displacement reached 25 mm with a corresponding load of 4 800 kN. From then on, the test was controlled by vertical displacement, and the applied load decreased with the increase in the out-of-plane displacement. The final crack patterns of specimen DW1 are shown in Figs. 4(a) and (b). Specimen DW1 failed due to concrete crushing in the top regions of the wall (see Fig. 5(a)) with a load of 4 400 kN and a corresponding out-of-plane displacement of 35 mm.

(a)

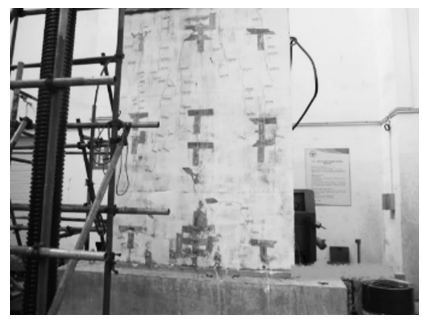

(b)

Fig. 4 Final crack patterns of specimen DW1. (a) Crack patterns and concretes crushed after loading; (b) Final crack patterns

(a)

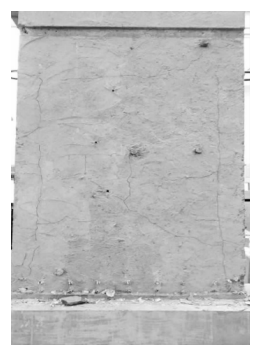

(b)

Fig. 5 Specimen DW2 after fire exposure. (a) Exposed side; (b) Unexposed side

Specimen DW2 has the same insulation thickness as DW1 but it was subjected to fire exposure on one side of the sandwich wall for approximately 120 min. During the fire test, the water inside the concrete changed into steam and escaped from the unexposed side of the sandwich wall. Moreover, significant pore pressure was induced by the vapor. The pore pressure increased continuously until it exceeded the tensile strength of the concrete, leading to concrete spalling (see Fig. 5(a)). As heating continued, water collected and moistened the unexposed surface. When the moisture dried out, horizontal and vertical cracks along the length of the steel bars were observed in the wall on the unexposed side (see Fig. 5(b)). When heating was finished, severe spalling of the concrete

caused by explosions on the exposed surface was observed, and the reinforcement was exposed to the air directly (see Fig. 5(a)).

After the heated wall cooled naturally, a vertical load was applied in the same way as for DW1. The first crack caused by the axial pressure was observed under a load of 750 kN at the top concrete beam. Vertical cracks in the upper part of the wall were found under a load of 1 200 kN on the unexposed surface. The original cracks caused by high temperature propagated into a series of transverse cracks under the axial load. With an increase of the external load, the number and width of the cracks in the specimen increased, so did the out-of-plane displacement of the wall. When the load reached 3 000 kN, vertical displacement control was applied to the specimen. Concrete-cover spalling and reinforcement buckling (see Fig. 6 (a)) were spotted under a load of 3 600 kN. A plurality of long cracks with a large width (approximately 1.5 mm) on the unfired surface was found when the load reached 3 750 kN. Along with a violent noise of "bang", the concrete at the top of the wall close to the bottom of the beam was crushed (see Fig. 6(b)) with a load of 3 800 kN. Soon afterwards, the load decreased as the out-of-plane displacement increased, and the test was terminated when the measured displacement at the top of the wall almost reached the range of the LVDTs. The final crack distribution of the unexposed side of specimen DW2 is shown in Fig. 6(c).

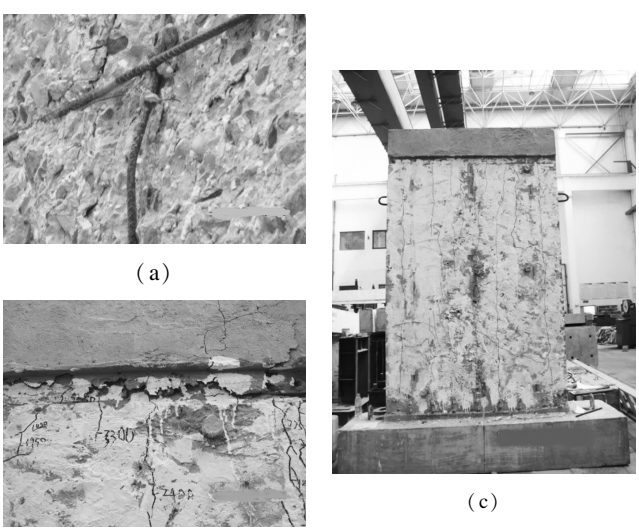

(a) (b) (c)

Fig. 6 Failure characteristics of specimen DW2. (a) Concrete cover spalling; (b) Reinforcement buckling; (c) Crack pattern on the unexposed side

Specimen DW3 is a normal-temperature specimen with an insulation thickness of 60 mm, and its other parameters are the same as those of specimen DW1. When the load reached 1 100 kN, the first crack occurred in the top concrete beam, and vertical cracks in the upper part of the wall were obtained under a load of 3 600 kN. The concrete beam at the top of the wall was crushed when the load increased to 4 000 kN, and the steel bars were exposed with a load of 4 090 kN (see Fig. 7(a)). The measured out-of-plane displacement at the top of the wall was close to 30 mm, and the widths of the main cracks on both sides of the wall reached approximately 2 mm. Fig. 7(b) shows the crack distribution in the top regions of the wall when it is destroyed.

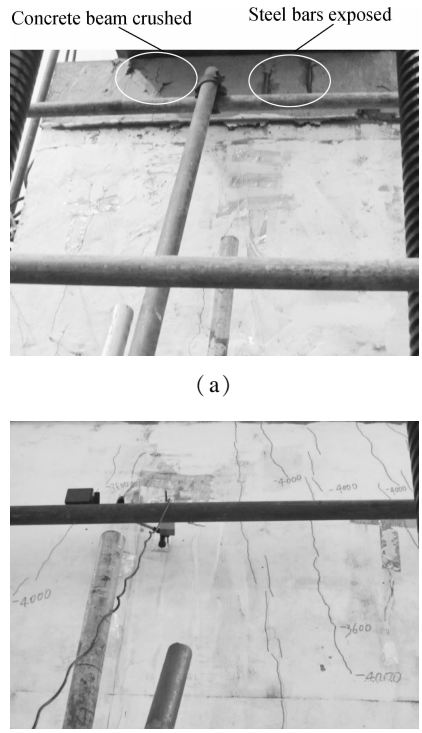

(a) (b)

Fig. 7 Failure characteristics of specimen DW3. (a) Concrete crushed and steel bars exposed; (b) Crack pattern

As for specimen DW2, one side of specimen DW4 was exposed to fire for 2 h in the fire furnace. The difference between the two specimens is that specimen DW4 has an insulation thickness of 60 mm, 20 mm thicker than that of specimen DW2. The damage of specimen DW4 was similar to that of specimen DW2. For example, the side subjected to fire exposure was seriously damaged (fine cracks in the unexposed side of the wall caused by high temperature were spotted), and concrete scaling and reinforcement exposure were observed (see Figs. 8(a) and (b)). Several cracks in the concrete beam at the top of the wall were first found under a load of 600 kN, and the first vertical crack on the unexposed side of the wall was observed when the load reached 1 050 kN. With the increasing load, transverse cracks began to appear in the unexposed surface, and the number and width of cracks at the top of the wall increased. The crack width was close to 1 mm when the load reached 2 400 kN. The ultimate load was obtained at an out-of-plane displacement of 34.9 mm with a load of 3 400 kN and the maximum crack width reached 1.5 to 2 mm. The test was finished when

the out-of-plane displacement at the top of the wall reached 40 mm. The failure characteristics of specimen DW4 are shown in Figs. 8(c) and (d).

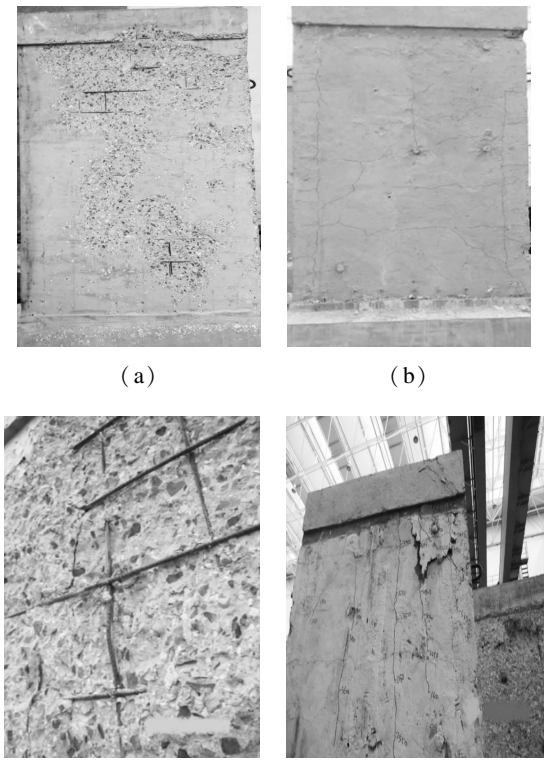

(a) (b) (c) (d)

Fig. 8 The characteristics of specimen DW4. (a) Exposed side post-fire; (b) Unexposed side post-fire; (c) Concrete cover spalling and reinforcement buckling after loading; (d) Crack patterns and concrete crushed on the unexposed side after loading

2.2 Axial compressive bearing capacity

Tab. 3 shows the axial compressive bearing capacities of the four specimens obtained from the test. As seen in Tab. 3, the bearing capacities of specimens DW2 and DW4, which have been exposed to fire for 2 h, are lower than those of conventional specimens DW1 and DW3. The axial compressive capacity of concrete specimens is primarily influenced by the compressive strengths of the concrete and the reinforcement. However, the compressive strength of concrete and the bond strength can be significantly reduced by elevated temperatures, and the yielding strength of the reinforcement will decrease as well[19]. The deterioration of the concrete, reinforcement and bond strength after fire exposure will decrease the axial compressive bearing capacity of the sandwich walls. Moreover, the temperatures of the unexposed and exposed surfaces are quite different, resulting in different degrees of damage to the wall. Therefore, the specimen is likely to suffer an eccentric compression load, and the stability of the specimen will be weakened, which decreases the axial compressive bearing capacity of the specimens. The axial compressive bearing capacities of specimens DW3 and DW4 are 14.8% and 10.5% lower, respectively, than those of specimens DW1 and DW2 because the compression strength of the EPS board is lower than that of concrete, whether subjected to fire exposure or not. Therefore, the larger the EPS used, the lower the axial bearing capacity of the specimen will be. Compared with that of specimen DW1, the axial bearing capacity of specimen DW2 decreased by 20.8%; the axial bearing capacity of specimen DW4 was 16.9% lower than that of specimen DW3 (less than 20.8%). The results indicate that the thicker the insulation layer, the more the axial compressive bearing capacity decreases, showing that the insulation layer has a good thermal insulation effect.

Tab. 3 The axial bearing capacities of the specimens

Specimen	Fire exposure time/min	Thickness of EPS board/mm	Axial bearing capacity/kN
DW1		40	4 800
DW2	120	40	3 800
DW3		60	4 090
DW4	120	60	3 400

2.3 Load-displacement curves

The axial load vs. out-of-plane displacement curves for the bottom, mid-depth and top of the walls are presented in Fig. 9, which highlights the comparison between the normal-temperature specimens and the post-fire specimens, and the different insulation layer thicknesses. It can be seen in Fig. 9 that the relationship between the load and displacement for all the specimens can be divided into three periods. During the first period, the load-displacement curves in the early stage of loading were nearly linear, the deflections increased with the increase in load. With the increase in external loading, an inelastic stage was reached. At this stage, the load increased slightly with a relatively significant increase in deflection, and the curves gradually bent toward the displacement axis. After the load exceeded the axial bearing capacity, the load decreased while deflections continued to increase. The stiffness of the specimens decreased with the increasing displacement, so did the modulus of elasticity of the concrete. Compared with those of the specimens at room temperature, the stiffness of the specimens exposed to fire decreased and the maximal displacement increased, indicating that the mechanical properties of the concrete sandwich walls post-fire exposure were reduced due to fire damage.

It can be seen in Fig. 9 that when the load was the same, a thicker insulation layer led to a larger out-of-plane displacement. Both the axial compressive bearing capacity and the stiffness of specimen DW3 were lower than those of specimen DW1. Similar relationships can be seen for specimens DW4 and DW2, illustrating that the axial compressive bearing capacity and stiffness decreased

with the increasing insulation layer thickness (whether exposed to fire or not). As the compressive strength and stiffness of the EPS board are lower than those of concrete, whether subjected to fire exposure or not, the larger the EPS used, the lower the axial compressive bearing capacity and stiffness of the specimen will be. Nevertheless, the axial bearing capacity and stiffness of the specimens exposed to fire decreased less because the insulation layer inhibited the stiffness reduction.

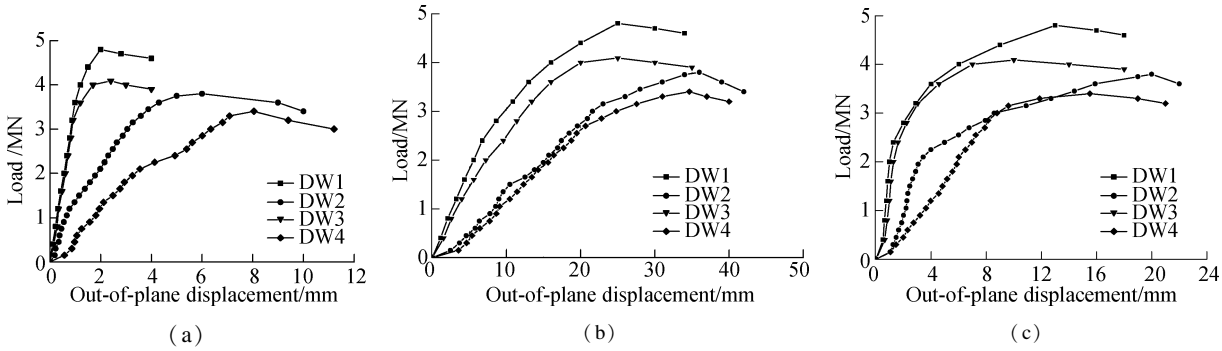

Fig. 9 Load-displacement curves of DW1 to DW4. (a) At the bottom; (b) At the mid-depth; (c) At the top

2.4 Comparison of the concrete strains

Fig. 10 shows the relationship between the axial load applied to the specimens and the strain of concrete at the bottom, mid-depth and top of the walls between the normal-temperature specimens and the post-fire specimens, and insulating layer thicknesses. In Fig. 10, we can see that the ultimate concrete strain of the post-fire specimens were larger than those of the normal-temperature specimens in the same position. Moreover, the concrete strain of the post-fire specimens were larger than those of the normal-temperature specimens in the same position when the load was at the same level. The strain distribution characteristics reveal that the deterioration of concrete and steel bars after fire exposure weakened the mechanical properties of the walls, resulting in larger axial strain in the concrete. Fig. 10 also shows that the thicker the insulation thickness, the larger the strain of concrete (whether the specimens were exposed to fire or not) is. However, the strain deviations of the post-fire specimens are smaller due to the fire resistance of EPS.

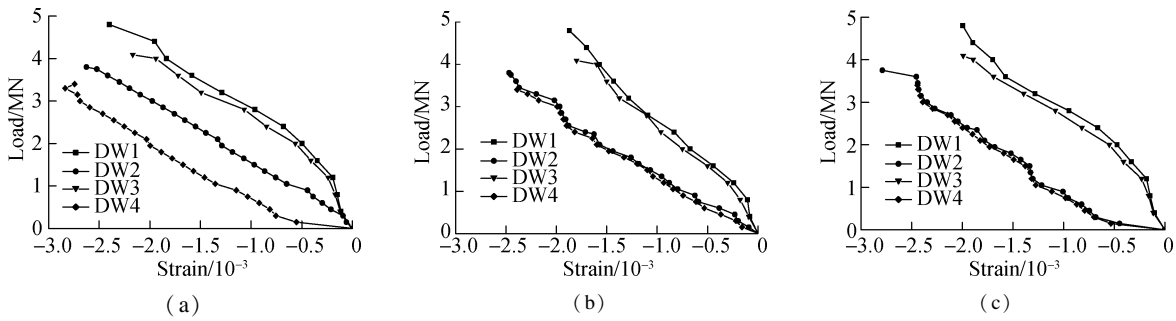

Fig. 10 Load-concrete strains curves of DW1 to DW4. (a) At the top; (b) At mid-depth; (c) At the bottom

2.5 Comparison of the reinforcement strains

The relationships between axial load and compression strains for the steel bars of the normal-temperature and post-fire specimens are given in Fig. 11. It can be seen that the compression strains of the steel bars of the four specimens are small at the initial loading stage. As there were few concrete cracks at the initial loading stage, the loads were primarily resisted by the concrete, and the distinction of the reinforcement strains of the four specimens were not obvious. With the increase in load, the reinforcement strain increments of the post-fire specimens were larger than those of the normal-temperature specimens since concrete cracks occurred earlier in the post-fire specimens. Compared with the specimens at room temperature, the strains of the post-fire specimens were much larger at the same position and same loading level. The primary reason for this is that elevated temperatures can damage the concrete and its reinforcement as well as its bond strength.

Fig. 11 also shows the comparison of the relationship between the axial load and reinforcement strains of specimens with different insulation layer thicknesses. It can be seen in Fig. 11 that the thicker the insulation layer, the larger the reinforcement strains at the same load level (whether the specimens were exposed to fire or not). As the compressive strength of the EPS board is lower than that of concrete, the larger the EPS used, the larger the

axial deformation of the specimen will be, resulting in a larger strain of the reinforcement.

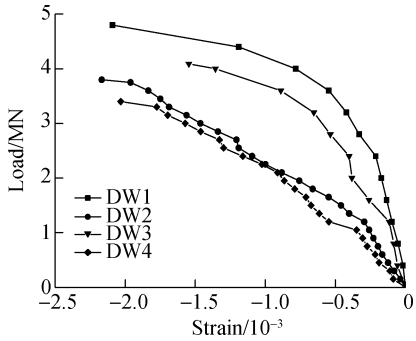

Fig. 11 Load-reinforcement strains curves

3 Conclusion

1) The deterioration of the concrete, reinforcement, and bond strength, as well as the probable eccentric compression load after elevated temperature exposure, resulted in lower axial compressive bearing capacities for the post-fire specimens than for the normal-temperature specimens. Compared with specimen DW1, the axial compressive bearing capacity of specimen DW2 decreased by 20.8%; the axial compressive bearing capacity of specimen DW4 was 16.9% lower than that of specimen DW3 (less than 20.8%). The thicker the insulation layer, the more the axial compressive bearing capacity decreased, showing that the insulation layer has a good thermal insulation effect.

2) Compared with those of the specimens at room temperature, the stiffness of the specimens exposed to fire decreased and the maximal out-of-plane displacement increased, indicating that damage to the concrete and EPS board in the fire caused a reduction in the stiffness of the sandwich walls. In addition, stiffness decreased with the increase in insulation layer thickness (whether exposed to fire or not) since the compressive strength and stiffness of the EPS board were lower than those of concrete. Nevertheless, the insulation layer inhibited the stiffness reduction, and the stiffness of the specimens exposed to fire decreased less.

3) The deterioration of materials post-fire exposure weakened the mechanical properties of the walls, resulting in larger concrete strains for the post-fire specimens than for the normal-temperature specimens at the same position when the load was at the same level. Whether the specimens were exposed to fire or not, the thicker the insulation thickness, the larger the strain of concrete. However, the strain deviations of the post-fire specimens were smaller due to the fire resistance of EPS.

4) Differentiating the reinforcement strains of the four specimens was not possible at the initial loading stage, as there were few concrete cracks. With the increasing load, the reinforcement strain increments of the post-fire specimens were larger than those of the normal-temperature specimens since concrete cracking in the post-fire specimens occurred earlier and elevated temperatures can increase damage to the concrete and the reinforcement as well as to the bond strength. In addition, the larger the EPS used, the larger the axial deformation of the specimen will be, resulting in larger strain of the reinforcement.

References

[1] Mousa M A, Uddin N. Structural behavior and modeling of full-scale composite structural insulated wall panels [J]. *Engineering Structures*, 2012, **41**:320 − 334. DOI: 10.1016/j.engstruct.2012.03.028.

[2] Mathieson H, Fam A. Axial loading tests and simplified modeling of sandwich panels with GFRP skins and soft core at various slenderness ratios[J]. *Journal of Composites for Construction*, 2015, **19**(2): 04014040. DOI:10.1061/(asce)cc.1943 − 5614.0000494.

[3] Abdolpour H, Escusa G, Sena-Cruz J M, et al. Axial performance of jointed sandwich wall panels[J]. *Journal of Composites for Construction*, 2017, **21**(4):04017009. DOI:10.1061/(asce)cc.1943 − 5614.0000785.

[4] Naito C,Hoemann J, Beacraft M, et al. Performance and characterization of shear ties for use in insulated precast concrete sandwich wall panels[J]. *Journal of Structural Engineering*, 2010, **138**(1): 52 − 61. DOI: 10.1061/(asce)st.1943-541x.0000430.

[5] Xiong J, Ghosh R, Ma L, et al. Bending behavior of lightweight sandwich-walled shells with pyramidal truss cores[J]. *Composite Structures*, 2014, **116**: 793 − 804. DOI:10.1016/j.compstruct.2014.06.006.

[6] Tomlinson D,Fam A. Analytical approach to flexural response of partially composite insulated concrete sandwich walls used for cladding [J]. *Engineering Structures*, 2016, **122**: 251 − 266. DOI:10.1016/j.engstruct.2016.04.059.

[7] Ricci I, Palermo M, Gasparini G, et al. Results of pseudo-static tests with cyclic horizontal load on cast in situ sandwich squat concrete walls [J]. *Engineering Structures*, 2013, **54**: 131 − 149. DOI:10.1016/j.engstruct.2013.03.046.

[8] Choi I, Kim J H, You Y C. Effect of cyclic loading on composite behavior of insulated concrete sandwich wall panels with GFRP shear connectors[J]. *Composites Part B: Engineering*, 2016, **96**:7 − 19. DOI:10.1016/j.compositesb.2016.04.030.

[9] Palermo M, Trombetti T. Experimentally-validated modelling of thin RC sandwich walls subjected to seismic loads[J]. *Engineering Structures*, 2016, **119**:95 − 109. DOI:10.1016/j.engstruct.2016.03.070.

[10] Palermo M, Ricci I, Silvestri S, et al. Preliminary interpretation of shaking-table response of a full-scale 3-storey building composed of thin reinforced concrete sandwich walls[J]. *Engineering Structures*, 2014, **76**:75 − 89. DOI:10.1016/j.engstruct.2014.06.024.

[11] Woltman G, Noel M, Fam A. Experimental and numerical investigations of thermal properties of insulated concrete sandwich panels with fiberglass shear connectors

[J]. *Energy and Buildings*, 2017, **145**: 22 - 31. DOI: 10.1016/j.enbuild.2017.04.007.
[12] Zhang L, Bai Y, Chen W, et al. Thermal performance of modular GFRP multicellular structures assembled with fire resistant panels[J]. *Composite Structures*, 2017, **172**: 22 - 33. DOI: 10.1016/j.compstruct.2017.03.076.
[13] Pereira D, Gago A, Proença J, et al. Fire performance of sandwich wall assemblies[J]. *Composites Part B: Engineering*, 2016, **93**: 123 - 131. DOI: 10.1016/j.compositesb.2016.03.001.
[14] Xiao J Z, Xie Q H, Li Z W, et al. Fire resistance and post-fire seismic behavior of high strength concrete shear walls[J]. *Fire Technology*, 2016, **53**(1): 65 - 86. DOI: 10.1007/s10694-016-0582-6.
[15] Xiao J Z, Li J, Jiang F. Research on the seismic behavior of HPC shear walls after fire[J]. *Materials and Structures*, 2004, **37**(8): 506 - 512.
[16] Go C G, Tang J R, Chi J H, et al. Fire-resistance property of reinforced lightweight aggregate concrete wall[J]. *Construction and Building Materials*, 2012, **30**: 725 - 733. DOI: 10.1016/j.conbuildmat.2011.12.081.
[17] Fernando P L N, Jayasinghe M T R, Jayasinghe C. Structural feasibility of expanded polystyrene (EPS) based lightweight concrete sandwich wall panels[J]. *Construction and Building Materials*, 2017, **139**: 45 - 51. DOI: 10.1016/j.conbuildmat.2017.02.027.
[18] Peng Y Y, Qian J R, Wang Y H. Cyclic performance of precast concrete shear walls with a mortar-sleeve connection for longitudinal steel bars[J]. *Materials and Structures*, 2016, **49**(6): 2455 - 2469. DOI: 10.1617/s11527-015-0660-0.
[19] Ghandehari M, Behnood A, Khanzadi M. Residual mechanical properties of high-strength concretes after exposure to elevated temperatures[J]. *Journal of Materials in Civil Engineering*, 2010, **22**(1): 59 - 64. DOI: 10.1061/(asce)0899-1561(2010)22:1(59).

预制复合保温墙体单面受火后轴压承载力试验研究

付 倩[1] 朱筱俊[2] 梁书亭[1] 杨 建[1] 李向民[3] 许清风[3] 高明珠[1]

([1] 东南大学土木工程学院, 南京 210096)
([2] 东南大学建筑设计研究院有限公司, 南京 210096)
([3] 上海市建筑科学研究院上海市工程结构安全重点实验室, 上海 200032)

摘要: 为了研究内、外页钢筋混凝土墙板、EPS 板及钢套筒连接件组成的预制复合保温墙体火灾后的轴压承载能力,对 4 个预制复合保温墙体试件(2 个常温试件及 2 个火后试件)进行了火灾后轴压承载力试验. 观察了其破坏形态、裂缝开展情况;测试了其轴压承载力、墙体面外位移、混凝土及钢筋应变. 试验结果表明:火后试件的抗压极限承载力均低于常温试件的极限承载力;保温层厚度 40 mm,降幅为 20.8%,厚度为 60 mm,降幅为 16.8%;火后墙体的最大平面外位移值明显比常温墙体大,在相同荷载作用下,保温层厚度越大,墙体的平面外位移越大;火后墙体的混凝土、钢筋应变总是比常温墙体的大,保温厚度较大墙体的混凝土、钢筋应变均大于保温层厚度较小墙体的应变.

关键词: 预制复合保温墙体; 膨胀聚苯乙烯板; 火灾; 保温层; 受火后; 轴压性能
中图分类号: TU317